Prediction and Measurement of Boundary Waves at the Interface Between LiNbO₃ and Silicon

Dorian Gachon, William Daniau, Emilie Courjon, Vincent Laude, Sylvain Ballandras, and Hicham Majjad

Abstract—Interface acoustic waves (IAWs) propagate along the boundary between two perfectly bonded solids. For a leakage-free IAW, all displacement fields must be evanescent along the normal to the boundary inside both solids, but leaky IAWs may also exist depending on the selected combination of materials. When at least one of the bonded solids is a piezoelectric material, the IAW can be excited by an interdigital transducer (IDT) located at the interface, provided one can fabricate the transducer and access the electrical contacts. We discuss here the fabrication and characterization of IAW resonators made by indirect bonding of lithium niobate onto silicon via an organic layer. In our fabrication process, IDTs are first patterned over the surface of a Y-cut lithium niobate wafer. A thin layer of SU-8 photo-resist is then spun over the IDTs and lithium niobate to a thickness below one micrometer. The SU-8-covered lithium niobate wafer then is bonded to a silicon wafer. The stack is subsequently cured and baked to enhance the acoustic properties of the interfacial resist. Measurements of resonators are presented, emphasizing the dependence of propagation losses on the resist properties. Comparison with theoretical computations based on periodic finite element/boundary element analysis allows for explanation of the actual operation of the device.

I. Introduction

WAFER bonding for piezoelectric substrates currently appears to be a key technology to manufacture passive devices for high-frequency signal processing. SAW devices typically have been used for the fabrication of frequency references, sensors, and filters. Several points related to aging, quality factor limitation, low-cost packaging, or surface pollution (electric, acoustic) have to be addressed in modern SAW devices. Interface acoustic waves (IAWs) are, at least in principle, able to push back these restrictions. IAWs, also named boundary waves, were first described by Stoneley [1]. Theoretical studies and the conditions of existence of IAW for some piezoelectric substrates have been reported [2], [3]. Analysis methods used for SAWs, i.e., the effective permittivity and

the harmonic admittance computed within the Blötekjaër approach [4] were extended to IAWs in classical piezoelectric cuts to estimate the phase velocity, attenuation, and electromechanical coupling of IAW at the interface between standard piezoelectric materials, i.e., quartz, lithium tantalate, and lithium niobate [5]. These first theoretical calculations more or less agree with Hashimoto's results computed in a very similar approach [6]. More accurate predictions were achieved using our periodic mixed finite element analysis/boundary element method (FEA/BEM) computation code to account for the actual shape of one transducer's period [7], [8]. Although this approach provides a better analysis of the actual device operation than the Blötekjaër approach [5], similar conclusions were deduced from these works.

Experimental results for IAWs were claimed to be obtained with a LiTaO₃ substrate covered with a thick silicon oxide layer [9]. However, we consider that because the higher interface between SiO₂/air or SiO₂/vacuum is seen by the waves, they are much closer to Sezawa modes than to actual IAWs. Note that other groups progress in the development of technological approach capable to provide true IAW devices [10], [11].

Wafer bonding is a promising alternative to the deposition of thick layers. The main problem in bonding pre-processed wafers is the effect of surface roughness. We report here on the design and fabrication of a device using a Y-cut lithium niobate (LiNbO₃) wafer bonded using a thin epoxy-based photo-resist layer (SU-8) to a silicon wafer [12]. The developed process exploits IC-compatible micro-machining technologies which, in our case, allow for batch fabrication of complete 3-inch wafers and wafer-level packaging. The presence of this adhesive layer between the LiNbO₃ substrate and the silicon wafer yields guiding conditions significantly different than the ideal wafer-to-wafer bounding hypothesis as considered in [5].

The first section of the paper shows theoretical work dedicated to understanding the waveguide operation, accounting for the presence of the SU-8 adhesive layer. Particularly, one can see the influence of the bounding thickness on the spectral density and the electromechanical coupling of the IAW guided at the interface. The following part presents technological developments used to build real devices (single-port synchronous resonators). The third section is dedicated to experimental measurements, emphasizing the pertinence of our theoretical analysis. As a conclusion, we propose new perspectives for IAW-based devices.
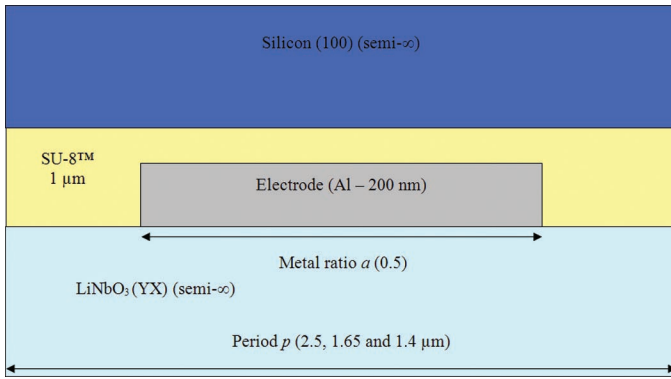
Fig. 1. One period of a LiNbO$_3$/SU-8/Si IAW structure with an aluminum electrode structured on the LiNbO$_3$ wafer. Indication of typical interface parameters considered both for computation and fabrication.

Fig. 2. Harmonic admittances computed using the Blötekjaër model, without and with the adhesive layer accounted for.

II. Theoretical Analysis

Fig. 1 shows a schematic view of the structure considered in the analytical simulations. The effect of an intermediate layer has been studied for such a structure, accounting for actually manufactured devices. We have adapted our periodic FEA/BEM code [7] to simulate acoustic radiations at both surfaces of the mesh, not only on one side as described in [7]. Although the general Lagrangian formulation of the problem remains the same as for standard surface waveguide simulation, particular care must be dedicated to the Green's function calculation to correctly account for the radiation direction in the BEM integrals. The boundary element integration then is achieved on each side of the mesh with the appropriate Green's function and the associated Bloch-Floquet development [7]. Note that the numbers of harmonics of the later development on each side of the mesh are independent and may be optimized for controlling the computation accuracy and/or duration. Basic principles of the modeling approach remain identical to those of [7].

Practically, the aluminum IDTs are deposited on the lithium niobate surface. Their actual thickness is not taken into account when simulating using the effective permittivity method [5]. The silicon wafer is assumed to be a (YX)-cut semi-infinite substrate, the SU-8 resist is 1 μm thick, the SiO$_2$ layer is a 360 nm thick, physical vapor deposited (PVD) layer, and the lithium niobate semi-infinite medium corresponds to a (YX)-cut. The physical constants (elastic, dielectric, and piezoelectric) of the various materials are well-known in the literature, except for the SU-8 resist. Although this resist is not dedicated to this kind of application, we intend to prove that it allows for manufacturing IAW test devices, even if this organic resist presents more acoustic losses than mineral materials. The SU-8 resist parameters (considered as an isotropic dielectric) are as follows:

- density: 1190 kg/m^3,
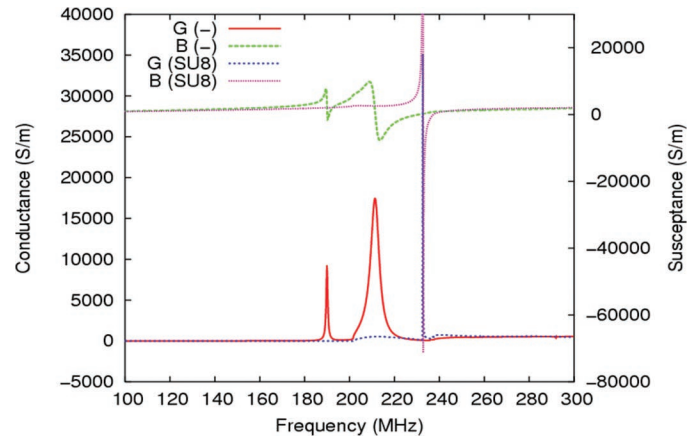- Young's modulus: 4.02 GPa,
- Poisson's ratio: 0.22,

- Dielectric constant: 3.

The Young's modulus is particularly low (nearly 50 times lower than the lithium niobate elastic constant c_{11}). SU-8 actually is far from rigid and has very low longitudinal and transverse acoustic velocities. The components of the SU-8 elastic tensor deduced from the above figures are: $c_{11} = 4.59$ GPa, $c_{12} = 1.29$ GPa, and thus $c_{66} = 1.65$ GPa.

Simulations were first carried out with different values of SU-8 losses to check the influence of this fundamental, but initially unknown, parameter. Losses are measured by a viscoelasticity coefficient η, so that an imaginary part equal to the viscoelasticity coefficient by the angular frequency product $\omega\eta$ [13] is added to the real (conservative) elastic constant.

Once these parameters are fixed, one can simulate the structure to be fabricated. A first computation is performed considering the assembly of (YX) silicon and (YX) LiNbO$_3$, but neglecting the presence of the adhesive SU-8 layer and considering the silicon to be perfectly dielectric. A shear-polarized interface mode is found with a phase velocity close to 4600 m·s^{-1}, exhibiting an electromechanical coupling of 4%. Considering the SU-8 layer in the computation process significantly changes the spectral behavior of the device, showing two modes contributing to the harmonic admittance at lower frequencies (phase velocities near 3800 m·s^{-1} and 4200 m·s^{-1}). The slowing down of the wave is easily explained by the presence of the SU-8 adhesive layer, for which bulk wave velocities are in the vicinity of 2000 m·s^{-1} (longitudinal) and 1200 m·s^{-1} (shear). Fig. 2 compares the two situations by superposing the corresponding harmonic admittances. Note that whatever the analysis conditions, the surface skimming bulk wave (SSBW) threshold of the LiNbO$_3$ persists in the present configuration, yielding an objective wave guidance limit.

One can observe the increase of losses caused by the adhesive layer, but also the strong value of the electromechanical coupling coefficient of the second mode (16%) that approaches the one of the leaky shear (SH)-type
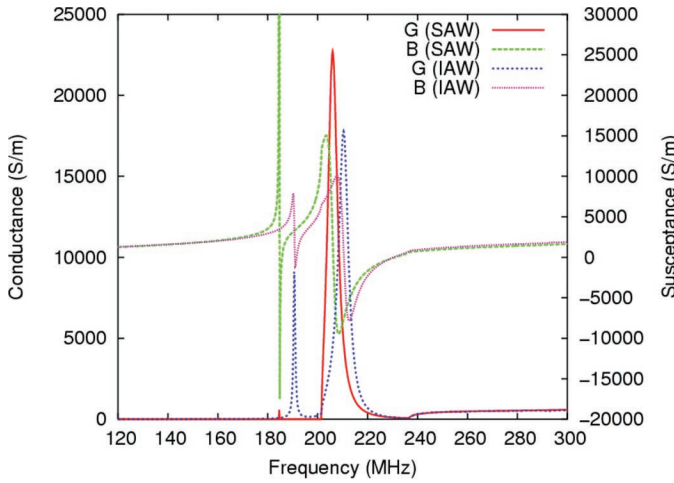
Fig. 3. Harmonic admittances computed using the Blötekjaër model. Comparison between IDT response on a semi-infinite (YX) LiNbO₃ wafer and at the silicon/niobate interface accounting for the adhesive layer.

Fig. 4. Harmonic admittances computed using the Blötekjaër model. Comparison between IDT response at the silicon/niobate interface for 2 different thicknesses of the adhesive layer.

Fig. 5. Implemented mesh for the simulation of interface wave excitation and guiding using our periodic FEA/BEM computation code. The boundary numbers correspond to the applied boundary conditions, i.e., a unit voltage excitation applied on boundary #1, periodicity conditions applied to boundaries #4 and #5, radiation in silicon applied to boundary #3, and radiation in lithium niobate applied to boundary #2.

Fig. 6. Comparison between harmonic admittances of the Si/SU-8/LiNbO₃ IAW guide provided by the Blötekjaër and the FEA/BEM analyses. The slight differences between the two results are due to mass loading accounted for in the FEA/BEM simulation (200-nm-thick Al electrode).

mode on the free surface of LiNbO₃ (YX) cut. We then compare both cases of SAW excitation at the surface of a semi-infinite (YX)-cut LiNbO₃ medium and at the Si/LiNbO₃ interface accounting for a 1-μm-thick adhesive layer. The corresponding harmonic admittances are reported in Fig. 3.

This plot tends to demonstrate that a wave exhibiting a polarization close to the one of the Rayleigh wave still exists but is accelerated at the silicon/niobate interface because of the influence of the silicon via the adhesive layer, whereas the leaky shear-horizontal wave of the free surface is slowed down because of the very small shear velocity in the SU-8 layer. Consequently, we assume that reducing the SU-8 layer first should increase the wave velocities, then reduce the electromechanical coupling for SH-type mode, and finally yield the spectral behavior of the device closer to the one without the adhesive layer. This is shown in Fig. 4, in which the SU-8 thickness has been reduced to 0.5 μm, and the corresponding admittance is compared with that of device with a 1-μm-thick SU-8 layer.

In Fig. 4 it clearly appears that the Rayleigh-like wave velocity increases and its coupling decreases when reducing the SU-8 thickness. At the same time, the quality factor Q of the SH-like mode tends to increase and its electromechanical factor decrease. Further reduction of the adhesive layer thickness is expected to cause Rayleigh-like wave to vanish, the admittance tending asymptotically toward that of the Blötekjaër analysis without SU-8 (c.f. Fig. 2).

To confirm these results, mainly concerning the nature of the waves and their polarization, we have computed the harmonic admittance considering the nominal adhesive layer thickness using our periodic FEA/BEM code [7] and compared it to the Blötekjaër analysis results. The implemented mesh is shown in Fig. 5, giving the definition of the computation conditions.

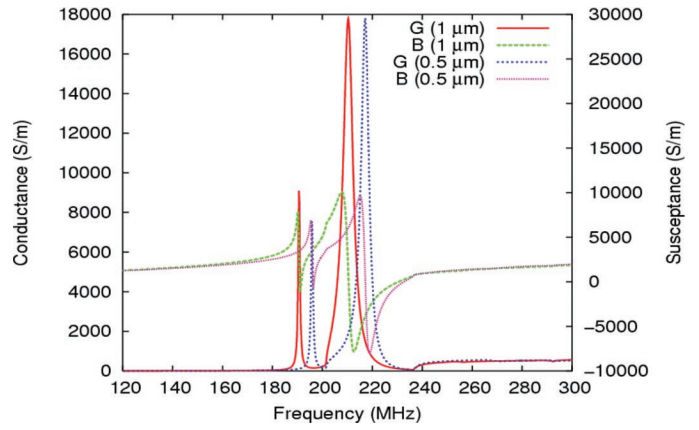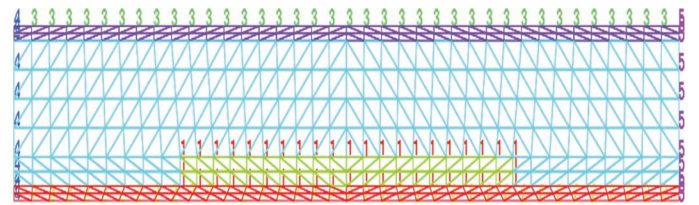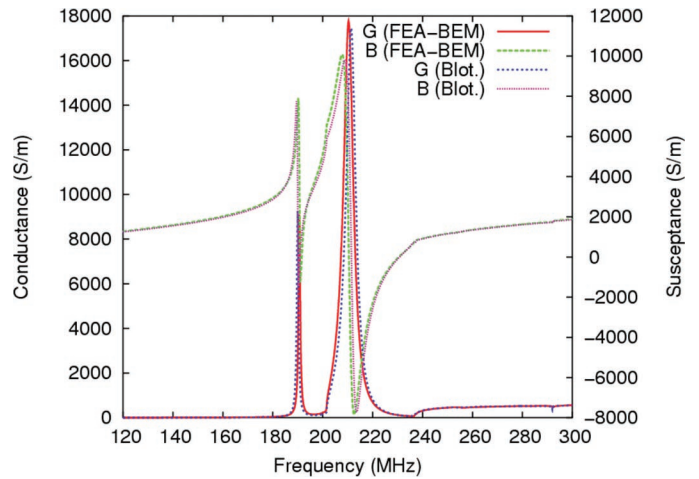Fig. 6 shows a very nice agreement between both theoretical approaches (as expected), the only difference being caused by the massive electrode taken into account in the FEA/BEM computation. Figs. 7 and 8 show deformed mesh sequences illustrating the Rayleigh-like and SH-like mode polarizations. They correspond to a decomposition of one time period in a 4-phase sequence ($\varphi = 0$ to $3\pi/4$), providing clear evidence for the previous analysis of the wave polarization. The iso-values correspond to displace-
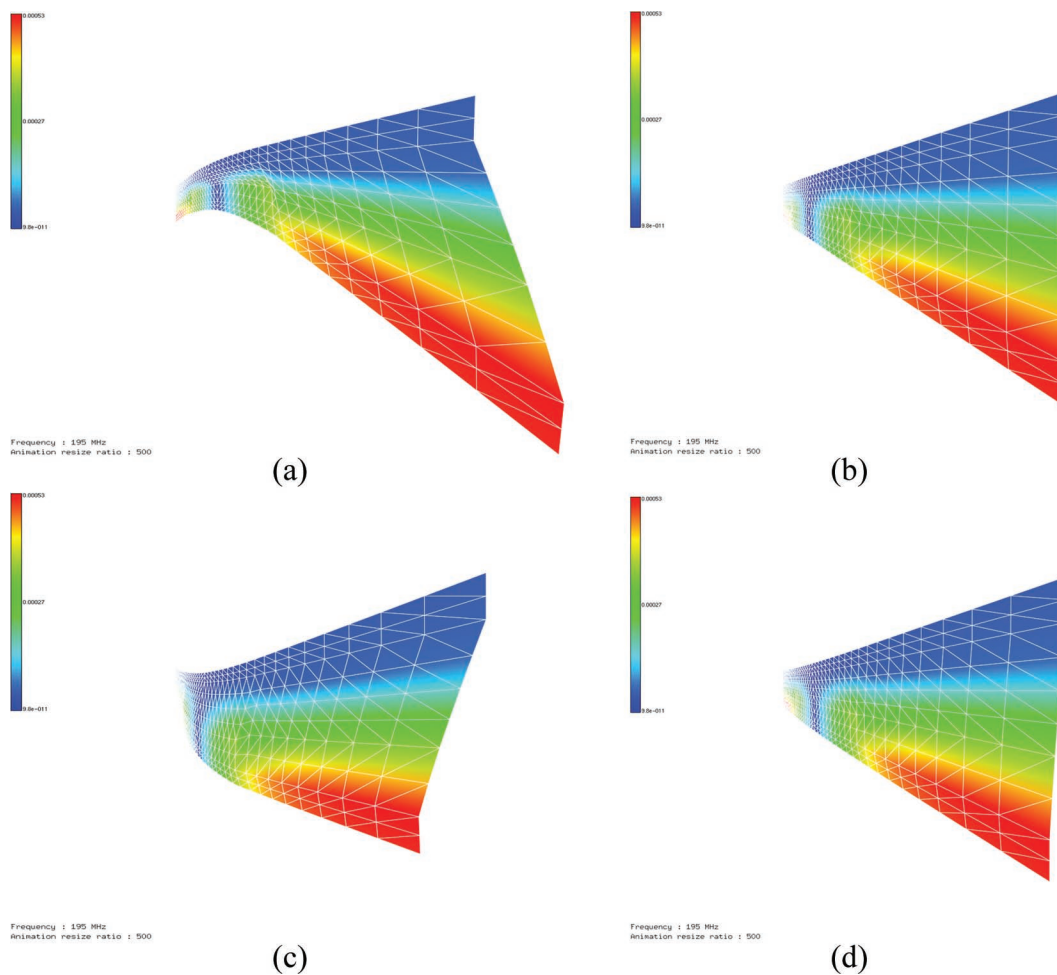
Fig. 7. Quadrature sequences of the dynamic deformation of the Rayleigh-like (elliptically polarized) mode: (a) $\varphi = 0$, (b) $\varphi = \pi/4$, (c) $\varphi = \pi/2$, (d) $\varphi = 3\pi/4$.

ment along x_1 (propagation direction). For both modes, the polarization is general, but one can easily recognize the dominance of elliptic (Fig. 7) and shear polarizations (Fig. 8).

III. IAW Device Fabrication

General wafer bonding technology can be divided into two main branches: direct bonding [12] and intermediate layer bonding [13]. Currently, wafer bonding of piezoelectric substrates receives a certain interest [14]. However, wafer surface waviness and roughness are critical issues in direct bonding. Therefore, a low-temperature bonding method using a photosensitive material as adhesive intermediate layer was developed in this work, based on chemical surface hydrophilization and the SU-8 resist. First, aluminum (Al) inter-digital transducers (IDT) are patterned on a lithium niobate wafer. An SU-8 layer is spun onto the LiNbO$_3$ wafer. A silicon wafer with wet-etched vias then is bonded onto the LiNbO$_3$ substrate. We also intend to demonstrate the interest in IAWs propagating on silicon-based compound substrate, assuming further

co-integration possibilities (acoustics and electronics). The fabrication and wafer bonding process are schematically summarized in Fig. 9.

The starting substrate is a 0.5-mm-thick 3-inch (YX)-cut LiNbO$_3$ wafer. A 220-nm-thick chromium-aluminum layer is sputtered onto the polished side of the wafer. The photo-resist then is spun to form a 1.4-µm thin layer, onto which pre-bake and hard-bake are applied. The mask used for the photolithography step has typical IDT patterns with a minimum finger width of 0.7 µm.

Once the resist developed, the metal layer is wet etched, providing the usual IDT's grating pattern. The LiNbO$_3$ substrate then can be passivated using a SiO$_2$ layer. This silicon dioxide layer is assumed to protect the aluminum resonators during the harsh cleaning treatment before bonding, but this step can be omitted because the SU-8 also acts as an insulating layer.

Before any bonding operation, vias must be achieved in the silicon plate to access the electrodes and to probe the device. The starting substrate is a 0.25-mm-thick 3-inch silicon wafer (100) covered with a uniform 1.4-µm thermal oxide layer. The SiO$_2$ layer then is etched locally using a standard lithography process, creating an *in situ* mask for
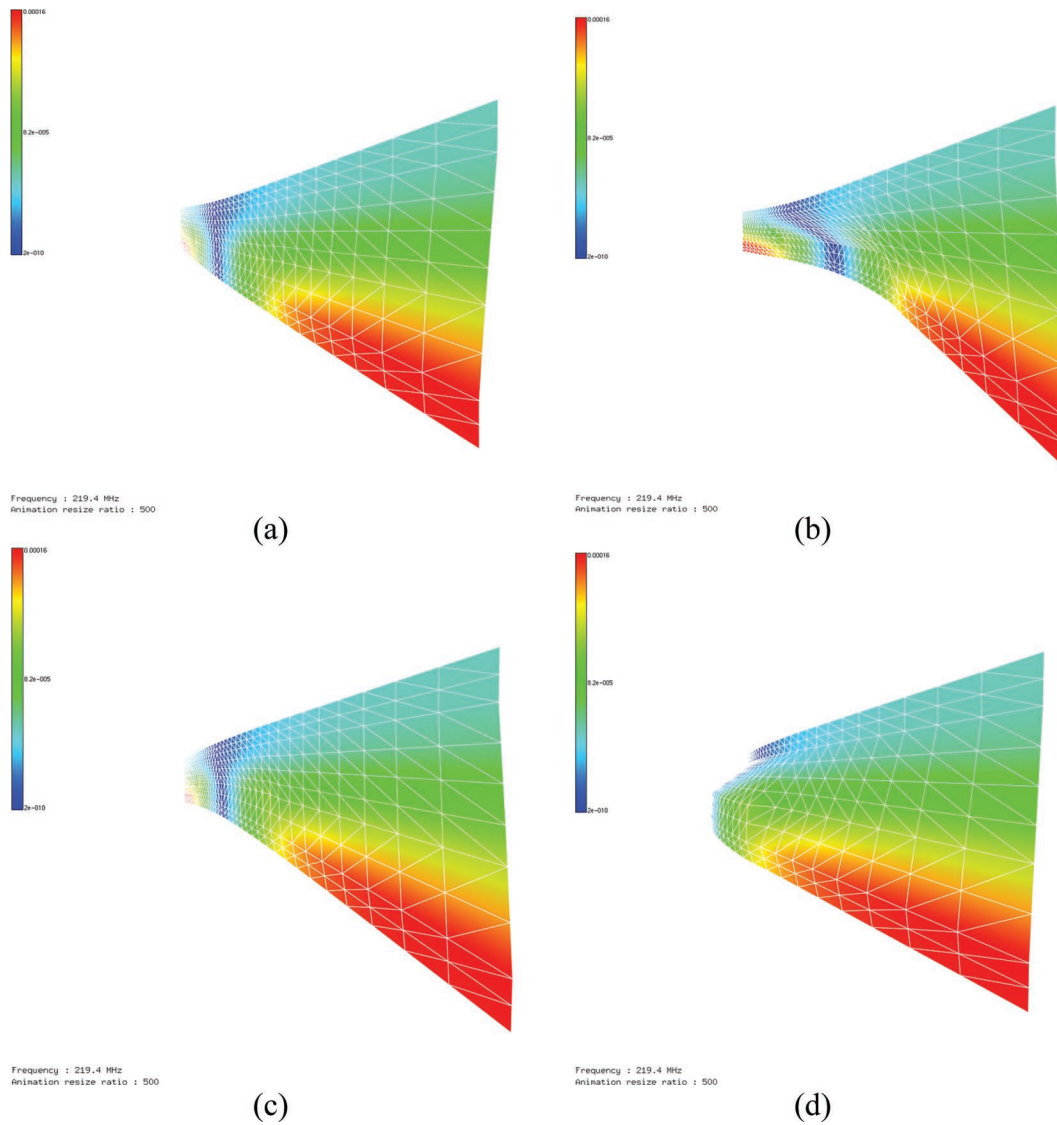
Fig. 8. Quadrature sequences of the dynamic deformation of the SH-like mode: (a) $\varphi = 0$, (b) $\varphi = \pi/4$, (c) $\varphi = \pi/2$, (d) $\varphi = 3\pi/4$.

potassium hydroxide (KOH) silicon anisotropic deep etch. Afterward, a re-oxidation of the wafer is done to obtain a SiO_2 thickness of 0.4 µm.

The wafers are cleaned to remove any kind of contaminants from the process. Hydrophilic treatment of the Si/SiO_2 is performed. The exact cleaning process is detailed in [9]. After this step, Epon SU8-2001 is conventionally spun on the $LiNbO_3$ wafer to obtain a 1-µm-thick layer. A 30-min relaxation time on a flat support is used to get an uniform coating on the wafer. The Si and $LiNbO_3$ wafers are aligned in an EVG 620 aligner (EV Group, St. Florian am Inn, Austria). The pair is subsequently transferred to an EVG 501 bonder (EV Group). The chamber of the wafer bonding machine is purged and evacuated to 10^{-3} mbar. The temperature rate in the heating process of the wafers is 1°C/min from room temperature to 65°C. Bonding occurred at 65°C under a pressure of about 11 Mpa (a 500 N force applied on a 3-inch wafer) for 1 h. After bonding, the stacked wafers are annealed at 65°C, for 1 h in at-mospheric N_2 ambiance to enhance the bonding strength. The temperature then is decreased to room temperature with a 1°C/min slope. Fig. 10 displays the result obtained after the low-temperature wafer bonding process.

Cross-sectional cuts are made with a dicing saw on the bonded device to analyze the bonding process, by imaging the bonded interface using scanning electron microscopy (SEM). An example of an SEM picture in Fig. 11, showing a very high quality bonding between the two wafers.

After the bonding process, SU-8 and SiO_2 layers still remain inside the via devised for electrical contact. SU-8 hashing and SiO_2 etching are performed in a PLASSYS re-active ion etching reactor (Marolles-en-Hurepoix, France). The remaining resist is dry etched with a gas mixture composed of oxygen and C_2F_6. We chose to dry etch SiO_2 using CHF_3 and C_2F_6 reactive ion etching (RIE). A thin resist layer is deposited on the $LiNbO_3$ back side to reduce spurious bulk acoustic wave (BAW) reflections. The stack then is diced for measurement.

LiNbO₃ PREPARATION

Al and Cr sputtering on LiNbO₃ wafer
Resist Lithography

Resist Development
Cr + Al etching
Resist Stripping

SiO₂ evaporation

SILICON PREPARATION

Lithography on Si/SiO₂ wafer
Backside resist protective layer

SiO₂ and Si wet etch

WAFER BONDING

SU-8 spinning for adhesive bonding

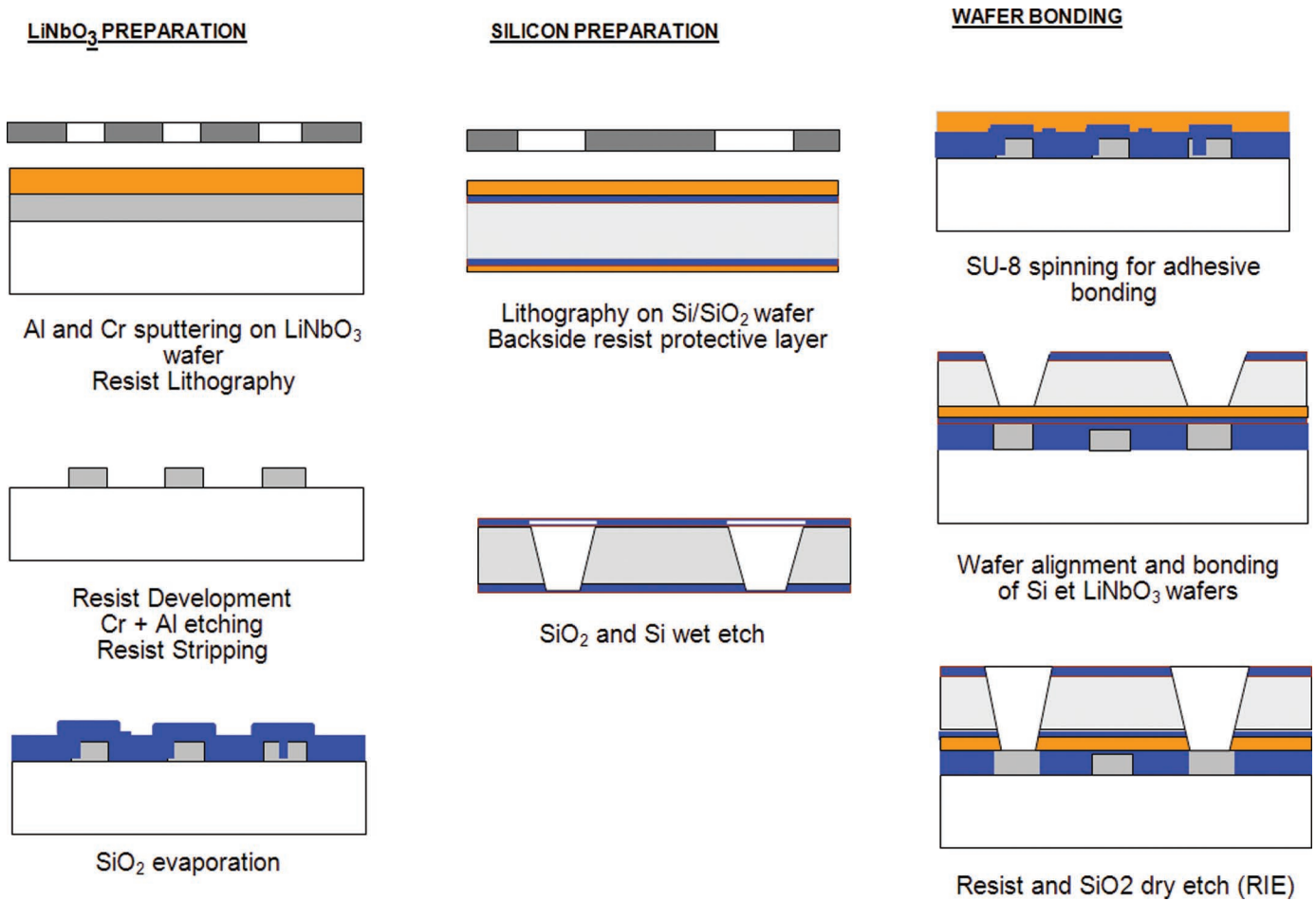Wafer alignment and bonding of Si et LiNbO₃ wafers

Resist and SiO2 dry etch (RIE)

Fig. 9. Flowchart for the adhesive wafer bonding process.

IV. MEASUREMENTS

The devices first have been characterized under RF probes connected to a Rohde & Schwarz ZVCE network analyzer (Munich, Germany). The wavelength of the tested devices has been set to 5, 3.3, and 2.8 μm, yielding a minimum strip width of 0.7 μm, near the very limit of our mask aligner. Most devices have been successfully tested but were also found to suffer from parasitic elements limiting the measurement quality. Therefore, we focus only on the 2.8 μm wavelength devices, providing the best experimental results and allowing for a reliable assessment and analysis of theory and experiment. Fig. 12 shows the experimental admittance of a typical one-port IAW resonator. We easily identify the two main contributions respectively at 1.39 and 1.62 GHz as the Rayleigh-like and the SH-like modes, corresponding to phase velocities close to 3900 and 4500 m·s⁻¹. The weak contribution near 1 GHz was not expected and must be identified using theoretical analysis. Fig. 13 shows the harmonic admittances computed with Blötekjaër and FEA/BEM approaches, providing a reliable prediction of the observed resonator responses. It must be indicated that this agreement was obtained after adjusting the SU-8 resist thickness from 1 μm down to 0.6 μm. Even though the experimental measurement is strongly perturbed by
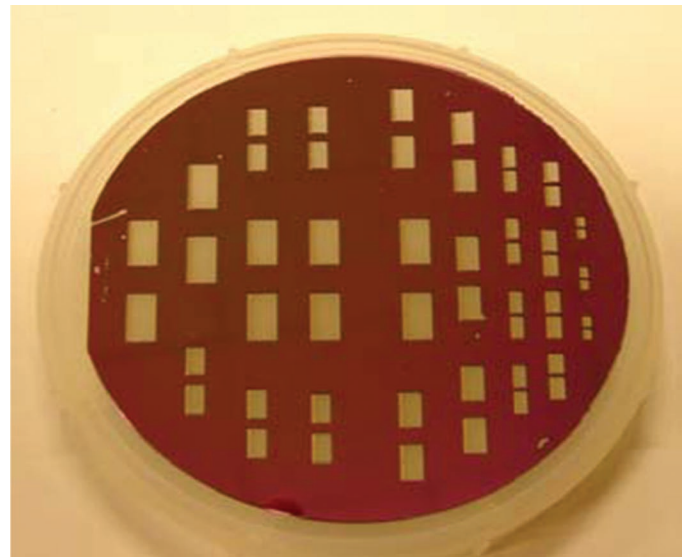

Fig. 10. Picture of the 3-inch bonded wafers (LN/Si) from the silicon side.

parasitic contributions, it can be emphasized that relative amplitudes of the different admittance contributions are correctly predicted by both theoretical approaches. We also point out that the electrode loading accounted for in the FEA/BEM computations was overestimated com-
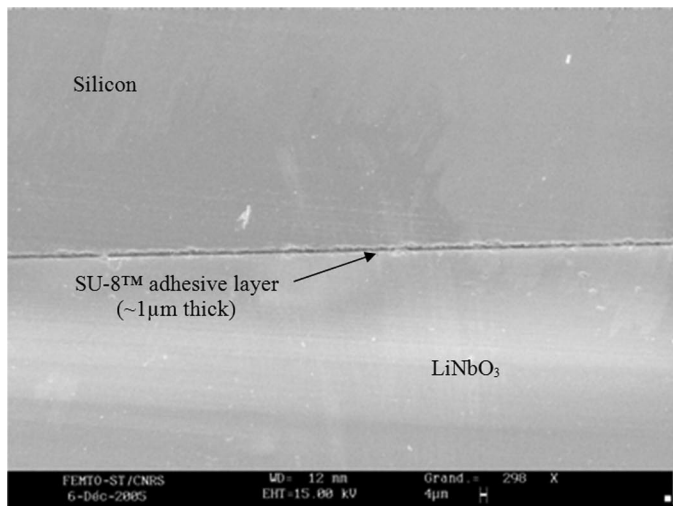
Fig. 11. Scanning electron micrograph of the stack after dicing. It shows the lithium niobate wafer, the adhesion interface, and the silicon substrate.
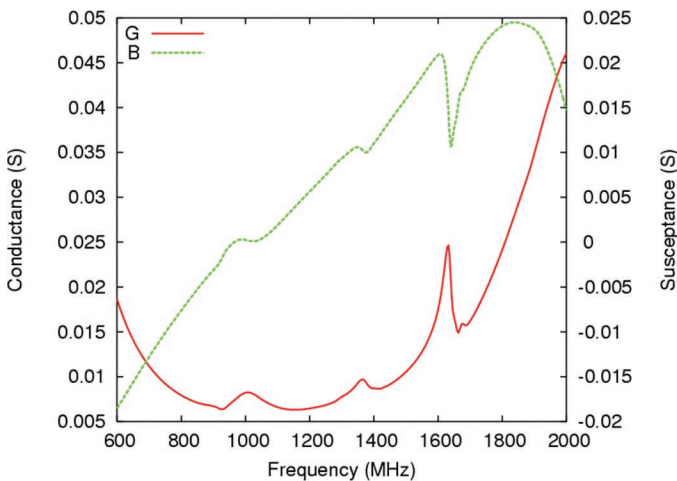

Fig. 13. Harmonic admittances of the 2.8-μm-wavelength IAW devices computed using the Blötekjaër and FEA/BEM approaches. The SU-8 resist thickness has been adjusted to fit the experimental results of Fig. 14. All the observed modes are predicted, but the electrode loading effects are overestimated by the FEA/BEM analysis.

Fig. 12. Experimental admittance of the 2.8-μm-wavelength IAW devices. The Rayleigh-like mode is found to propagate near 3900 m·s^{-1} whereas the SH-like mode exhibits a phase velocity close to 4500 m·s^{-1}.

Fig. 14. Polarization of the first (1 GHz) contribution, corresponding to a weakly coupled pure SH-like mode mainly localized within the SU-8 layer (isovalues are along the normal to the saggital plane).

pared with experimental and Blötekjaër analysis results. The sensitivity of the device response to the interface parameters thus suggests the need for a perfect control of the resonator fabrication to reach the level of agreement between theory and experiment usually met for SAW devices. Nevertheless, the FEA/BEM analysis allows a reliable identification of the mode polarizations. Figs. 14, 15, and 16 show the dynamically deformed mesh (for $\varphi = 0$) of the three observed admittance peaks. The first (1 GHz) contribution corresponds to a weakly coupled pure SH-like mode mainly localized within the SU-8 layer. The existence of this mode strongly depends on the SU-8 thickness and it tends to vanish when the resist layer is thicker than 0.8 μm. The second (1.39 GHz) contribution consists of a combination of a weak shear displacement with a strong elliptic motion, corresponding to the so-called Rayleigh-like contribution. Finally, the third (1.6 GHz) contribution, corresponds to a strongly coupled SH-like mode with
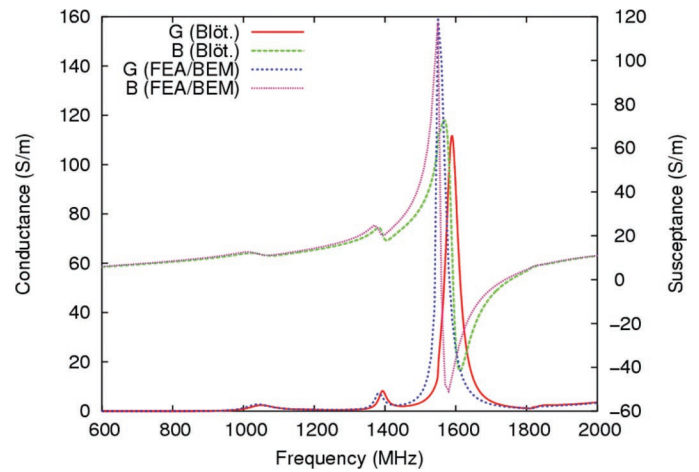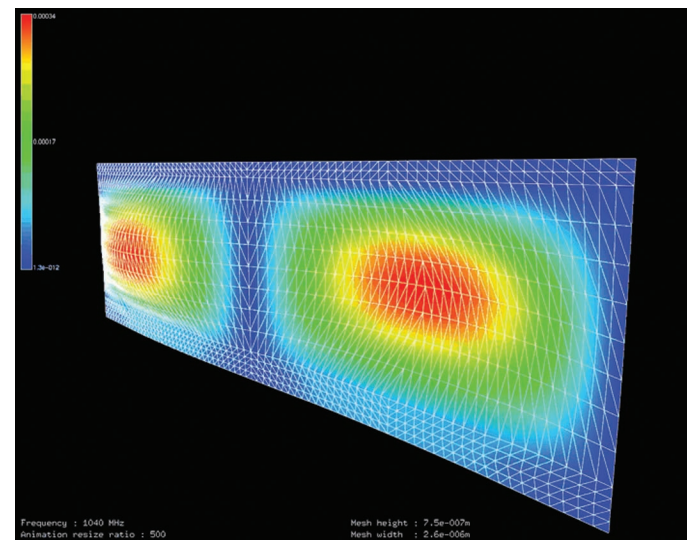
a small elliptic residual motion. In comparison with the first shear contribution, the mode distribution along the interface height corresponds to a whole sine alternation of the displacement normal to the saggital plane. However, there is no obvious harmonic relation between the two modes. For the two latter modes, the vibration is, of course, stronger near the LiNbO$_3$ medium because it is the actual location of the vibration source.

V. Conclusion

A theoretical analysis of the operation of IAW has been proposed to describe the characteristics of a waveguide composed of a silicon wafer and a lithium niobate wafer

Experiments are ongoing to increase device frequencies up to 2 GHz.

Although it was clearly demonstrated that waves can be excited and propagate at the interface between lithium niobate and silicon, it is also clear that this particular combination of materials with the bonding technique implemented cannot give rise to any practical application. Consequently, investigations are under way to decrease losses caused by the adhesive wafer bonding by using harder layers obtained, for instance, by spin-on-glass (SOG). The extension of the developed processes to other piezoelectric substrates such as lithium tantalate is also planned.
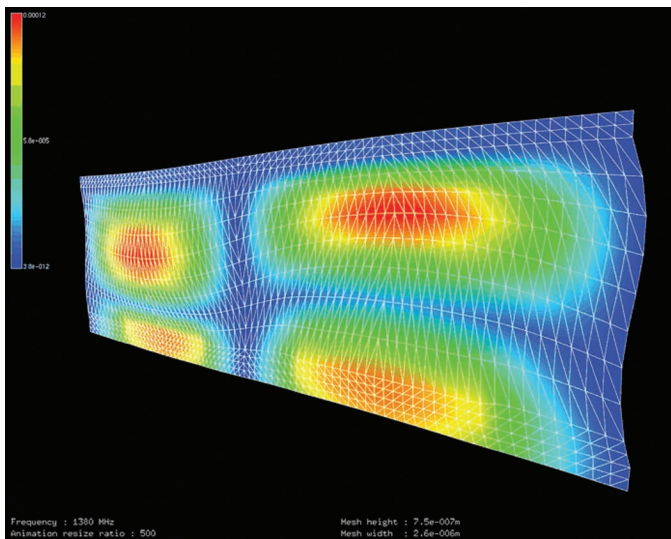

Fig. 15. Polarization of the second (1.39 GHz) contribution. The mode consists of a combination of a weak shear displacement with a strong elliptic motion (isovalues are along the normal to the saggital plane).
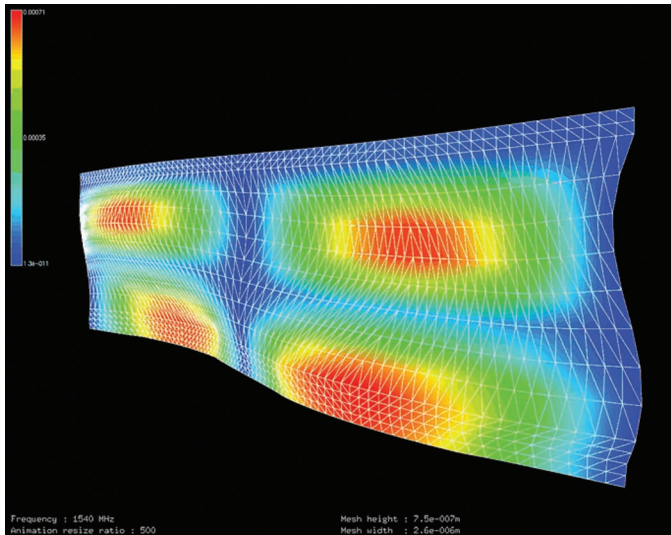

Fig. 16. Polarization of the third (1.6 GHz) contribution, corresponding to a strongly coupled SH-like mode with a small elliptic residual motion (isovalues are along the normal to the saggital plane).

bonded together using an adhesive layer, accounting for the presence of the excitation/detection electrode grating. Two modes are guided at the interface, the first being close to the free-surface Rayleigh wave atop $LiNbO_3$ and the second exhibiting a quasi-shear polarization. A low-temperature wafer hetero-bonding process of lithium niobate onto silicon also has been achieved, exploiting a thin spin-coated SU-8 film as an adhesive layer. It is the first experimental demonstration of interface acoustic wave devices made with this wafer bonding technique and operating at frequencies higher than 1 GHz. It is found that the presence of an adhesive layer between the $LiNbO_3$ wafer and the silicon wafer leads to strong losses of the IAW modes for any practical use, but allows for the excitation of a highly coupled SH-like mode ($K_s^2 > 10\%$).

REFERENCES

[1] R. Stoneley, "Elastic waves at the surface of separation of two solids," *Proc. R. Soc.*, vol. A106, pp. 416–428, 1924.

[2] C. Maerfeld and P. Tournois, "Pure shear surface wave guided by the interface of two semi-infinite media," *Appl. Phys. Lett.*, vol. 19, pp. 117–118, 1971.

[3] Y. Shimizu and T. Irino, "Stoneley waves propagating along an interface between piezoelectric material and isotropic material," in *Proc. IEEE Ultrasonics Symp.*, 1983, pp. 373–376.

[4] K. Blötekjaer, K. A. Ingebrigtsen, and H. Skeie, "A method for analysing waves in structures consisting of metal strips on dispersive media," *IEEE Trans. Electron. Dev.*, vol. 20, no. 6, pp. 1133–1138, 1973.

[5] S. Camou, V. Laude, T. Pastureaud, and S. Ballandras, "Interface acoustic waves properties in some common crystal cuts," *IEEE Trans. Ultrason. Ferroelectr. Freq. Control*, vol. 50, no. 10, pp. 1363–1370, 2003.

[6] K. Y. Hashimoto, T. Yamashita, and M. Yamaguchi, "Highly piezoelectric shear-horizontal-type boundary waves," *Jpn. J. Appl. Phys.*, vol. 36, pp. 3057–3059, 1997.

[7] S. Ballandras, R. Lardat, M. Wilm, Th. Pastureaud, A. Reinhardt, N. Champavert, W. Steichen, W. Daniau, V. Laude, R. Armati, and G. Martin, "A mixed finite element/boundary element approach to simulate complex guided elastic wave periodic transducers," *J. Appl. Phys.*, vol. 105, no. 1, art. no. 014911, 2009.

[8] S. Clatot, V. Laude, A. Reinhardt, M. Wilm, W. Daniau, S. Ballandras, R. Lardat, and M. Solal, "Sensitivity of interface acoustic waves to the nature of the interface," in *Proc. IEEE Ultrasonics Symp.*, 2003, vol. 2, pp. 2126–2129.

[9] K. Yamanouchi, K. Iwahashi, and K. Shibayama, "Piezoelectric acoustic boundary waves propagating along the interface between SiO_2 and $LiTaO_3$," *IEEE Trans. Sonics Ultrason.*, vol. 25, no. 6, pp. 384–389, 1978.

[10] N. Tai, T. Omori, K. Hashimoto, and M. Yamaguchi, "Acoustic boundary wave devices in Si/inlaid-IDT/$LiNbO_3$ structure," in *Proc. 27th Symp. Ultrasonic Electronics*, Nagoya, Japan, 2006, pp. 111–112.

[11] K. Bhattacharjee, S. Zghoon, and A. Shvetsov, "Packageless SAW devices with isolated layer acoustic waves (ILAW) and waveguiding layer acoustic waves (WLAW) ," in *Proc. IEEE Int. Frequency Control Symp. Joint With European Frequency Time Forum*, Geneva, Switzerland, 2007, pp. 135–140.

[12] D. Gachon, E. Courjon, G. Martin, L. Gauthier-Manuel, J.-C. Jeannot, W. Daniau, and S. Ballandras, "Fabrication of high frequency bulk acoustic wave resonator using thinned single-crystal lithium niobate layers," *Ferroelectrics*, vol. 362, pp. 30–40, 2008.

[13] S. Ballandras, A. Reinhardt, A. Khelif, M. Wilm, V. Laude, W. Daniau, and V. Blondeau-Pâtissier, "Theoretical analysis of damping effects of guided elastic waves at solid/fluid interfaces," *J. Appl. Phys.*, vol. 99, art. no. 054907, 2006.

[14] C. T. Pan, P. J. Cheng, M. F. Chen, and C. K. Yen, "Intermediate wafer level bonding and interface behavior," *Microelectron. Reliab.*, vol. 45, no. 3–4, pp. 657–663, 2005.

[15] T. Ohtsuchi, M. Sugimomto, T. Ogura, Y. Tomita, O. Kawasaki, K. Eda, "Shock sensors using direct bonding of $LiNbO_3$ crystals," in *Proc. IEEE Ultrasonics Symp.*, 1996, pp. 331–334.

Dorian Gachon was born in France in 1980. He graduated from the Université de Franche-Comté, Besançon France, with the Ph.D. degree in the field of time and frequency in 2008. His interests are in the development of high stability and spectral purity oscillators for X-band applications.

William Daniau was born in 1965 in St-Jean-de-Mont, France. He received his Ph.D. degree from the Université de Franche-Comté in engineering science in 1991 in time-and-frequency applications. He joined the Centre National de la Recherche Scientifique in 1992 as a Research Engineer. After assuming the responsibility of Laboratoire de Physique et Métrologie des Oscillateurs's (LPMO) clean room facilities for 7 years (1993 to 2000) and participating in numerous technological developments dedicated to 3-D micro-fabrication (silicon micromachining, photolithography techniques, LIGA and assimilated processes, etc.), he has joined the Acoustics and Microsonics group [LPMO department of Franche-Comté Electronique, Mécanique, Thermique et Optique–Sciences et Technologies (FEMTO-ST) from 2000 to 2007], for which the main activities concern surface acoustic wave devices for signal processing (filters, sources, etc.) and sensor applications as well as ultrasonic transducers for medical imaging and non-destructive evaluation. He was promoted to first row Research Engineer in 2003. Its main interests concern the development of new technologies for microsonics; in the last few years, he opened its fields of activity to include acoustoelectronics-oriented software development and he is in charge of the software packages and computer resources of the group.

Emilie Courjon obtained an Engineer Degree in biomedical instrumentation from the Institut Superieur d'Ingenieur de Franche-Comté (ISIFC) in Besançon, France, in 2004. Since 2005, she has been working as an engineer in the Franche-Comté Electronique, Mécanique, Thermique et Optique–Sciences et Technologies (FEMTO-ST) in Besançon in the acoustic team and she started a Ph.D. thesis in 2006 in collaboration with the Centre National de la Recherche Scientifique (CNRS). Her research focuses on a new type of acoustic transducers based on periodically poled ferroelectric domains. She also works on annular array transducers for ophthalmology.

Vincent Laude holds a Ph.D. degree in optics and photonics from Paris-Sud University (1994) and a habilitation degree from the Franche-Comté University (2002). He was a researcher at the Thomson-CSF Corporate Research Laboratories from 1995 to 1999, and with Thomson-CSF Microsonics in 2000. He was nominated to be a permanent researcher at the Centre National de la Recherche Scientifique (CNRS) in October 2000, and a research director in 2006. His research focuses on the propagation of elastic and acoustic waves in micro- and nano-structures, and notably on acoustic band gap materials (aka phononic crystals). He is also interested in highly confined acousto-optical interactions, for instance in phoXonic crytals and fibers. He was the head of the Laboratoire de Physique et Métrologie des Oscillateurs's (LPMO) research department of the Franche-Comté Electronique, Mécanique, Thermique et Optique–Sciences et Technologies (FEMTO-ST) Institute for 2006 and 2007, and is presently the head of the Micro Nano Sciences & Systems (MN2S) research department.

Sylvain Ballandras was born in Strasbourg, France, in 1965. He joined the Centre National de la Recherche Scientifique (CNRS) in 1991, after receiving his Ph.D. degree in engineering sciences from the Université de Franche-Comté. Until 1995, he was working on SAW devices, but he was also involved in microtechnologies. He has initiated the development of a finite element analysis package devoted to acoustic transducers and also new researches on miniaturized transducers. During 1997, he completed a one-year industrial training project in SAW industry (TMX, Sophia Antipolis, France). In 2003, he was promoted to Research Director at the CNRS. In 2008, his group joined the Time-Frequency Department of Franche-Comté Electronique, Mécanique, Thermique et Optique–Sciences et Technologies (FEMTO-ST), Besançon. Its present scientific developments concern fundamentals in acoustics and guided propagation as well as technologies dedicated to acousto-electronic devices and systems, focused on sources, filters, and sensors. Dr. Ballandras also benefits from the 25.2 agreement of the French Research Rules to join the head staff of the firm SENSeOR developing acousto-electric sensor systems.

Hicham Majjad received a Ph.D. degree in engineering sciences from Franche-Comté University in 2001. He was a postdoctoral researcher at the Angström Laboratory, Uppsala University, Sweden, from 2002 to 2004 where he was working on ion track lithography. Then he was working on interface acoustic waves at the Franche-Comté Electronique, Mécanique, Thermique et Optique–Sciences et Technologies (FEMTO-ST) Institute. He is now the head of STnano, a nanotechnology facility which belongs to the Centre National de la Recherche Scientifique (CNRS) and Strasbourg University. His research is to develop new processes for molecular electronic and magnetic tunnel junctions at the Institut de Physique et Chimie des Matériaux de Strasbourg (IPCMS).